Nuclear Physics A553 (1993) 297c–308c
North-Holland, Amsterdam

NUCLEAR
PHYSICS A

Quasi-Elastic Electron Scattering off Nuclei

L. Lapikás

National Institute for Nuclear Physics and High-Energy Physics (NIKHEF, section K),
P.O. Box 41882, 1009 DB Amsterdam, The Netherlands

Abstract

A survey is given of results of electron-induced quasi-elastic proton knockout experiments. We present results of experimental investigations of the (e,e'p) reaction-mechanism, among which are a separation of three of the four structure functions, and the determination of the momentum-transfer dependence of the cross section. Furthermore, the experimental momentum distributions are compared to Distorted Wave Impulse Approximation calculations that employ bound-state wave functions evaluated in a mean-field potential. The mass- and energy-dependence of the deduced spectroscopic strengths are discussed on the basis of modern calculations of the nuclear response that include short-range correlations.

1. INTRODUCTION

For the description of nuclear ground-state wave functions the mean-field approximation has been extensively used as a basis for calculations. In this approximation the motion of the nucleons in the nucleus is in zeroth order described by their interaction with a mean-field potential, which generally is taken to be a self consistent approximation of the sum of all mutual nucleon-nucleon interactions. The difference between this mean-field potential and the actual sum of nucleon-nucleon interactions is known as the residual interaction, and to a certain extent its influence can be included in the wave function via perturbation theory. These so-called correlations have been extensively debated after their early theoretical treatment by Jastrow in 1955 [1]. Various refinements have since been made involving several sophisticated approaches and at present one is able to calculate correlated many-body wave functions "exactly" for the few-body systems ($A \leq 4$) [2,3] and for infinite nuclear matter [4,5], starting from realistic nucleon-nucleon interactions. For finite ($A > 4$) nuclei most calculated wave functions are still based on a mean-field description, i.e. the leading contribution in a series of multi-particle correlations. The next order diagrams have been approached with a variety of techniques, most of which suffer from the inherent difficulty of treating the short-range and tensor part of the nucleon-nucleon interaction adequately. Several attempts to construct correlated many-body wave functions for finite nuclei, based on a realistic nucleon-nucleon interaction, have recently commenced (see e.g. [6,7]). These calculations are approaching the nuclear wave functions by either extending variational and Green's functions Monte-Carlo techniques from few-body nuclei to more complex systems, or by the application of correlated basis functions, currently employed in infinite nuclear-matter calculations, for finite nuclei. The present question of interest is how one can experimentally establish the limits of this mean-field description of nuclear wave functions.

The first quantitative comparisons between predictions of mean-field theory and experimental data have been made for the ground-state charge-density distributions of nuclei as determined from elastic electron scattering [8]. It was found that various types of Hartree-Fock (HF) calculations with semi-realistic nucleon-nucleon interactions could accurately describe the densities in the surface region of the nucleus, but generally overestimate the density in the

interior by up to 20%, an effect that was attributed to the lack of correlations in the HF wave functions. At present one still does not avail of many-body wave functions, based on realistic nucleon-nucleon interactions, that adequately explain the nuclear density in the interior.

Another experimental indication for strong correlations between nucleons in complex nuclei comes from inclusive quasi-elastic electron scattering. Measurements of the longitudinal part of the inclusive quasi-elastic response function in (e,e') experiments show a quenching with respect to the Coulomb Sum-Rule (for a review see [9]), which seems to increase with mass number The reduction of the longitudinal strength has been qualitatively explained for the few-body systems by assuming that the strength is spread out over a large energy domain due to NN-correlations [10,11]. However, for heavier nuclei this effect fails to explain the data.

Both the elastic and the quasi-elastic (e,e') experiments involve observables sensitive to contributions from the wave functions of all nucleons. For a more detailed study of the limitations of mean-field theory one also needs information on the individual nucleon orbitals. Such information is e.g. obtained from high-multipolarity transitions in (e,e') reactions [12,13]. The strength of these transitions appears to be quenched by a factor of about 0.6 with respect to the mean-field value. It was suggested that this quenching is a sign of reduced occupancies of single-particle orbitals and therefore primarily a manifestation of the influence of correlations that could not be accounted for within the framework of mean-field theory with phenomenological interactions. However, a direct relationship between these data and correlations is difficult to establish because of the presence of configuration-mixing and core-polarisation effects, which are hard to calculate accurately.

The most direct way to obtain information on individual nucleon wave functions is by nucleon knockout experiments, the basic ingredients of which are described in section 2. As the reliability of the results obtained with this reaction depends crucially on an accurate understanding of the reaction mechanism, we first discuss this subject in section 3. The determination of the nuclear structure information is discussed in section 4. Here the structure of the spectral function , i.e. the meeting place between theory and experiment is discussed for complex (A>4) nuclei. Results for the few-body systems are presented elsewhere in this proceedings [14,15].

2. DESCRIPTION OF THE QUASI-ELASTIC (e,e'p) REACTION

The formalism of the (e,e'p) reaction has been described in detail elsewhere [16], so only some major features are presented here. In plane-wave Impulse Approximation (PWIA) the energy ω and momentum $\mathbf{q}$ lost by the electron are transferred to a proton with binding (missing) energy E_m and (missing) momentum $-\mathbf{p}_m$, which then leaves the nucleus with momentum $\mathbf{p}' = \mathbf{q} - \mathbf{p}_m$ and kinetic energy $T_{p'}$ (see fig. 1). In PWIA the coincidence cross section can be written as

$$\frac{d^6\sigma}{de'\,dp'} = K\sigma_{ep}S(p_m,E_m), \tag{2.1}$$

where K is a kinematical (phase-space) factor, σ_{ep} is the (off-shell) electron-proton cross section, e.g. the current-conserving σ_{ep}^{ccl} from de Forest [17], and $S(p_m,E_m)$ is the spectral function, i.e. the probability to find in the parent nucleus a proton with binding energy E_m and momentum p_m. For the transition to a discrete state with quantum numbers $\alpha = \{nlj\}$ one can write

$$S(p_m,E_m) = \rho_\alpha(p_m)\delta(E_m-E_\alpha), \tag{2.2}$$

where the momentum density

$$\rho_\alpha(p_m) = \left|\Phi_\alpha^{if}(p_m)\right|^2 = \left|\int \left\langle \Psi^f_{A-1}\middle|\Psi^i_A\right\rangle e^{i\mathbf{p}_m\mathbf{r}}d\mathbf{r}\right|^2 \tag{2.3}$$

is the Fourier transform squared of the overlap between the initial and final nuclear state, which

is often called the bound-state wave function (BSWF). In the independent-particle shell model (IPSM) this BSWF is replaced by the single-particle or mean-field wave function $|\alpha>$. More generally, it can be identified with a quasi-particle wave function.

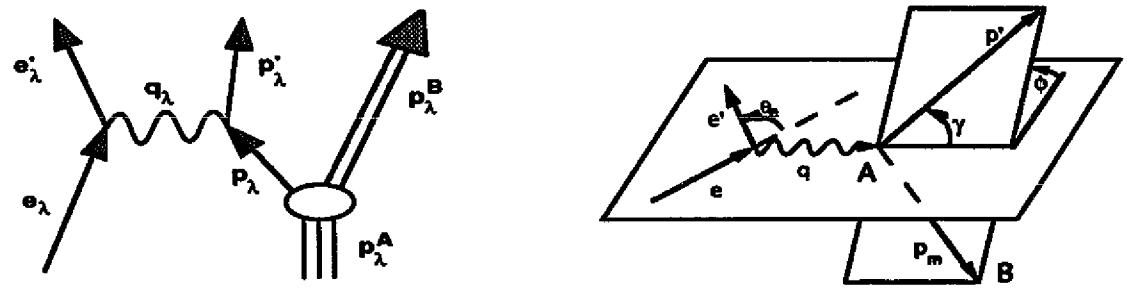

Fig. 1. Left panel : one-photon exchange diagram for the reaction A(e,e'p)B in Plane Wave Impulse Approximation. The symbols represent four-vectors. The electromagnetic field of the virtual photon $Q=-q\lambda=-(e\lambda - e'\lambda)$ is represented by the wavy line. The bound proton p_λ is knocked out of the nucleus A through the interaction with this field and subsequently detected ($p'\lambda$) in coincidence with the scattered electron $e'\lambda$. The energy and momentum of the bound proton $p\lambda=-(E_m,p_m)$ follow directly from the reconstructed invariants of the reaction: missing energy $E_m=e_0+p^A{}_0-e'_0-p'_0-p^B{}_0$ and missing momentum $\mathbf{p_m}=\mathbf{e}-\mathbf{e'}-\mathbf{p'}$. Right panel : definition of the kinematic planes entering in the description of the reaction according to eq. (3.1). The angle between the beam and the scattered electron is denoted by θ_e, the angle between the momentum transfer $\mathbf{q}$ and the emitted proton by γ, and the angle between the scattering plane (e,e') and the reaction plane (q,p') by ϕ.

If the final-state interaction is taken into account, the ejected proton is not in a free state but in a scattering state, described for instance by an optical-model (OM) wave function. In the actual calculations (referred to as Complete Distorted Wave Impulse Approximation (CDWIA)) the Coulomb distortion of the electron waves is also included [18,19]. For a comparison between experiment and theory we therefore define experimental momentum distributions by $\rho^{exp}(p_m) \equiv \sigma^{exp}/K\sigma_{ep}{}^{cc1}$ and compare these with analogously defined calculated momentum distributions $\rho^{CDWIA}(p_m) \equiv \sigma^{CDWIA}/K\sigma_{ep}{}^{cc1}$. The main assumptions in this formalism are that the virtual photon couples to a bound proton in the same way as to a free proton (Impulse Approximation) and that the final-state interaction effects between the outgoing proton and the residual nucleus can be described by an OM wave function. Implicit in the latter is that the photon has coupled to the knocked-out proton (no two-step knock-out).

3. REACTION MECHANISM TESTS

In order to investigate the validity of the description of the reaction mechanism we rewrite the coincidence cross section (eq. 2.1) in the more general form [20]

$$d^6\sigma/de'dp' = K\sigma_{Mott}\{W_L + \varepsilon^{-1} W_T + W_{TT}\cos 2\phi + \sqrt{(1+\varepsilon^{-1})}\, W_{LT}\cos\phi \}, \qquad (3.1)$$

where $\varepsilon^{-1} = 1+ 2(q^2/Q^2)\tan^2(\theta_e/2)$ is the virtual photon polarization and ϕ the angle between the reaction plane and the plane through $\mathbf{q}$ and $\mathbf{p'}$ (see fig. 1). The W_i's (i=L, T, TT, LT) are generalized structure functions that depend on $\mathbf{p_m}$, E_m, $\mathbf{q}$ and $\mathbf{p'}$, and that contain the nucleon elastic form factors $G_E(Q^2)$ and $G_M(Q^2)$. Below we describe three separate studies that have been carried out of the key elements in this description.

3.1 Ratio of transverse and longitudinal structure functions.

Since the interference structure functions W_{TT} and W_{LT} are proportional to the sine of γ, the angle between $\mathbf{q}$ and $\mathbf{p'}$, they do not contribute to the cross section in (anti) parallel ($\mathbf{q}//\mathbf{p'}$) kinematics (i.e. for $\gamma=0$ or π). Hence at a chosen Q^2 the longitudinal and transverse structure

functions can be determined from a Rosenbluth separation, i.e. by carrying out two measurements at the same value of (p_m,E_m) for different values of ε (i.e. of the combination E_o and θ_e). The ratio of structure functions, defined as

$$R_G = \frac{2M_p}{Q}\sqrt{\frac{W_T(Q^2)}{W_L(Q^2)}} \xrightarrow{\text{PWIA}} \frac{G_M(Q^2)}{G_E(Q^2)} \tag{3.2}$$

can then be used to study the validity of the Impulse Approximation, which predicts $R_G=\mu_p$ in the plane-wave case. In fig. 2 the results for R_G are shown for (e,e'p) experiments on ^{2}H [21], ^{6}Li [22,23], ^{12}C [24] and ^{40}Ca [25]. The ratio's were corrected for final-state interaction and Coulomb-distortion effects, and in the cases of ^{2}H and ^{40}Ca for the contributions of meson-exchange currents [21,26], which influence the transverse response function. These latter corrections were no larger than 5 %, and therefore will not affect our conclusions as they are believed to be of similar size for ^{6}Li and ^{12}C. The figure illustrates that after inclusion of these effects the data are well described with the ratio of the free nucleon form factors $G_E(Q^2)$ and $G_M(Q^2)$.

It should be noted that the present results apply to transitions to valence states below the two-nucleon emission threshold. Above this threshold two-nucleon emission is known [27,28] to contribute differently to the transverse and longitudinal structure functions, and therefore to obscure an unambiguous interpretation of the data in terms of one-nucleon knockout, which is the basis for eq. (3.2). For the few-body systems ^{3}He and ^{4}He measurements of R_G have been performed at Saclay [14,29]. The latter experiment seems to indicate an anomalous ratio of transverse and longitudinal structure functions when compared to calculations due to Laget [29]. However, recent calculations by Buballa et al. [30] are in agreement with the Saclay ^{4}He data, thus confirming our conclusions.

3.2 Momentum-transfer dependence of the cross section

The Q-dependence of the reaction cross section can be studied in two ways. Since one wants to exclude structure effects as much as possible in this study one should determine the response for a single transition at a fixed missing momentum p_m, i.e. the spectral function $S(p_m,E_m)$ should be constant (apart from distortion effects). Hence, $|\mathbf{p}_m| = |\mathbf{q}-\mathbf{p}'|$ should be constant, while $|\mathbf{q}|$, and therefore Q, varies. To realise this one can either choose : *i) parallel kinematics* with the consequence that $|\mathbf{p}'| = |\mathbf{q}| - |\mathbf{p}_m|$ varies and thus the final-state interaction, which depends on $T_{p'}$, changes simultaneously with Q. This approach was taken for the measurements on ^{4}He [31] and ^{90}Zr [25]; *ii) non-parallel kinematics*, where $|\mathbf{p}'|$ is fixed, but the angle γ between $\mathbf{q}$ and $\mathbf{p}$ varies such that $|\mathbf{p}_m|$ stays constant. This approach was taken for the measurement on ^{40}Ca [25].

The results of both approaches have been collected in fig. 3, where the ratio

$$R_Q = \sigma^{exp}(Q^2) / \sigma^{CDWIA}(Q^2) \tag{3.3}$$

is displayed as a function of Q^2. In the CDWIA calculations for the measurements on ^{40}Ca and ^{90}Zr we chose a normalization obtained from forward angle measurements at low Q in separate (e,e'p) experiments [32,33], while for ^{4}He the DWIA calculation employed the Illinois [3] theoretical wave functions. Because the employed CDWIA formalism contains a non-relativistic current operator, which causes a Q-dependent deviation of the electron-proton cross section compared to the Rosenbluth cross section, we corrected for this deficiency by dividing the calculated cross sections by a factor $\sigma_{ep}^{CDWIA}/\sigma_{ep}^{cc1}$, where σ_{ep}^{CDWIA} is the electron-proton cross section contained implicitly in the CDWIA code and σ_{ep}^{cc1} is the off-shell electron-proton cross section proposed by de Forest [17]. In all cases we also corrected for the contribution of meson-exchange currents [26], the size of which is indicated by the shaded area in fig. 3. The data shown pertain to the ground-state transition in the reaction ^{4}He(e,e'p), the sum of five strong discrete transitions ($1d_{3/2}$, $2s_{1/2}$, and $1d_{5/2}$) in the reaction ^{40}Ca(e,e'p)^{39}K and the sum of four strong discrete transitions ($2p_{1/2}$, $1g_{9/2}$, $2p_{3/2}$ and $1f_{5/2}$) in the reaction ^{90}Zr(e,e'p)^{89}Y.

From fig. 3 we conclude that in the Q^2-range up to 0.35 $(GeV/c)^2$ there is no significant deviation of the cross section from the Impulse Approximation provided that meson-exchange contributions are taken into account. Obviously, it will be very interesting to pursue these types of experiments to higher momentum transfer, where alternative descriptions like those involving a modification of the electromagnetic form factors of bound nucleons caused by the nuclear medium [20] or colour transparency effects [34] may become detectable.

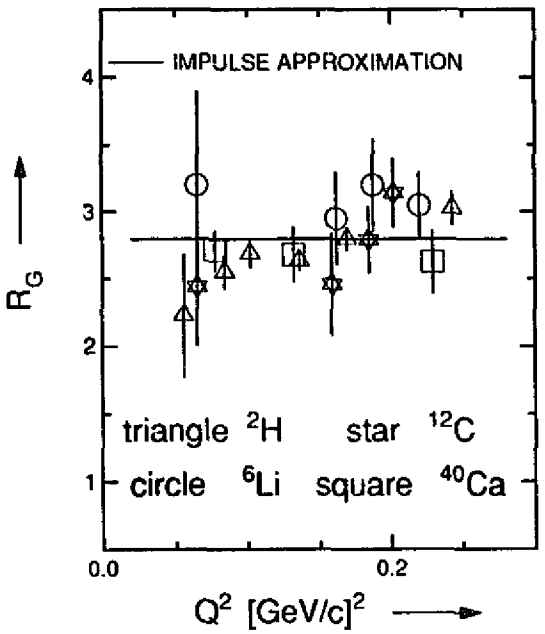

Fig. 2. Experimental values for R_G (see eq. 3.2) as a function of four-momentum transfer squared Q^2 for transitions to discrete states in the reaction (e,e'p) on ^{2}H [21], ^{6}Li [22,23], ^{12}C [24] and ^{40}Ca [25]. The data were corrected for proton and electron distortion effects within the CDWIA framework. The solid line represents the Impulse Approximation value for R_G . In addition the data for ^{2}H and ^{40}Ca were corrected for the effects of meson-exchange currents [21,26].

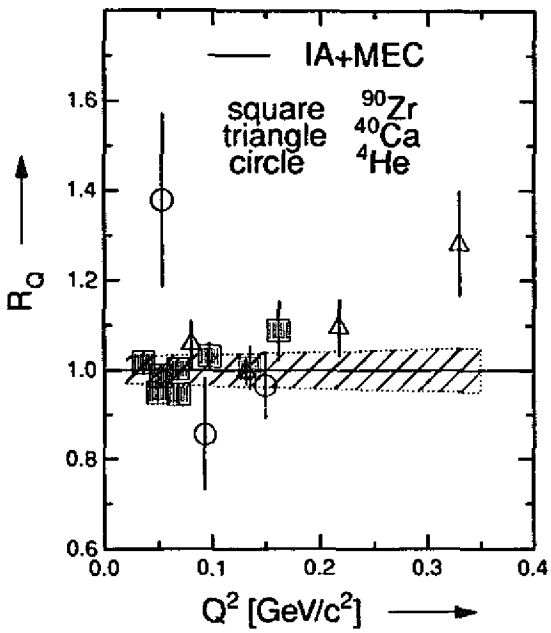

Fig. 3. Ratio R_Q of experimental and calculated CDWIA cross sections (see text for normalisation) for the reaction (e,e'p) on ^{4}He (open circles, [31]), ^{40}Ca (open triangles, [25]), and ^{90}Zr (solid squares, [25]) as a function of momentum transfer Q^2. The shaded area represents the size of the employed [26] corrections for the contributions of meson-exchange currents (MEC). The solid line represents the expected value for Impulse Approximation (IA) plus MEC.

3.3 The longitudinal-transverse interference structure function

As evident from eq. (3.1) the longitudinal-transverse interference structure function W_{LT} can be determined experimentally from two separate measurements of the coincidence cross section at out-of-plane angles $\phi=0$ and $\phi=\pi$, while all other kinematical parameters are kept the same. From such measurements, where one observes the proton **p'** both at the left and at the right side of the momentum transfer (**q**) direction, respectively, one easily determines W_{LT} via

$$W_{LT} = \frac{\sigma(\phi = 0) - \sigma(\phi = \pi)}{2K\sqrt{1-\varepsilon^{-1}}\,\sigma_{Mott}} \qquad (3.4)$$

These separations have been carried out at Saclay [35] for the reaction ^{16}O(e,e'p) and at NIKHEF for the reactions ^{2}H(e.e'p)n [36], ^{16}O(e,e'p)^{15}N [37], and ^{40}Ca(e,e'p)^{39}K [38]. The resulting structure function f_{01} ($=-W_{LT}12\pi^2\alpha/Q^2$) for deuterium is shown in fig. 4 as a function of missing momentum, together with a non-relativistic calculation by Arenhövel

[39] that includes final-state interaction and the contribution of meson-exchange diagrams, and a relativistic calculation by Hummel and Tjon [40] that includes the final-state interaction. There is a clear preference for the relativistic approach although the size of the systematic errors, indicated by the shaded area, prevents us from fully excluding the non-relativistic calculation.

For the reactions $^{16}O(e,e'p)^{15}N$ and $^{40}Ca(e,e'p)^{39}K$ we show the longitudinal-transverse structure functions for knockout from orbitals with $j=l\pm1/2$, together with CDWIA calculations employing bound-state wave functions and spectroscopic factors determined in separate experiments in parallel kinematics [41,33]. For the ground-state transitions ($1p_{1/2}$ for ^{16}O and $1d_{3/2}$ for ^{40}Ca) we observe good agreement between experiment and theory, whereas the absolute values of the experimental W_{LT} for $1p_{3/2}$ and $1d_{5/2}$ knockout are significantly overestimated by the theory. It remains to be investigated whether this discrepancy can be explained by e.g. relativistic effects like those observed in the case of the deuterium experiment [42] or by meson-exchange contributions [26].

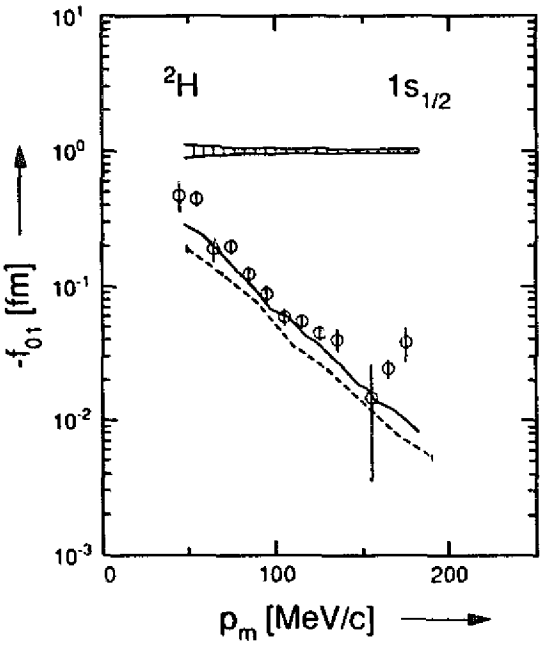

Fig. 4. Experimental values [36] for the longitudinal-transverse interference structure function f_{01} for the reaction $^2H(e,e'p)n$, compared to calculations in a non-relativistic (dashed, [39] and relativistic framework (solid, [40]). The shaded area indicates the size of the systematic uncertainties on the data.

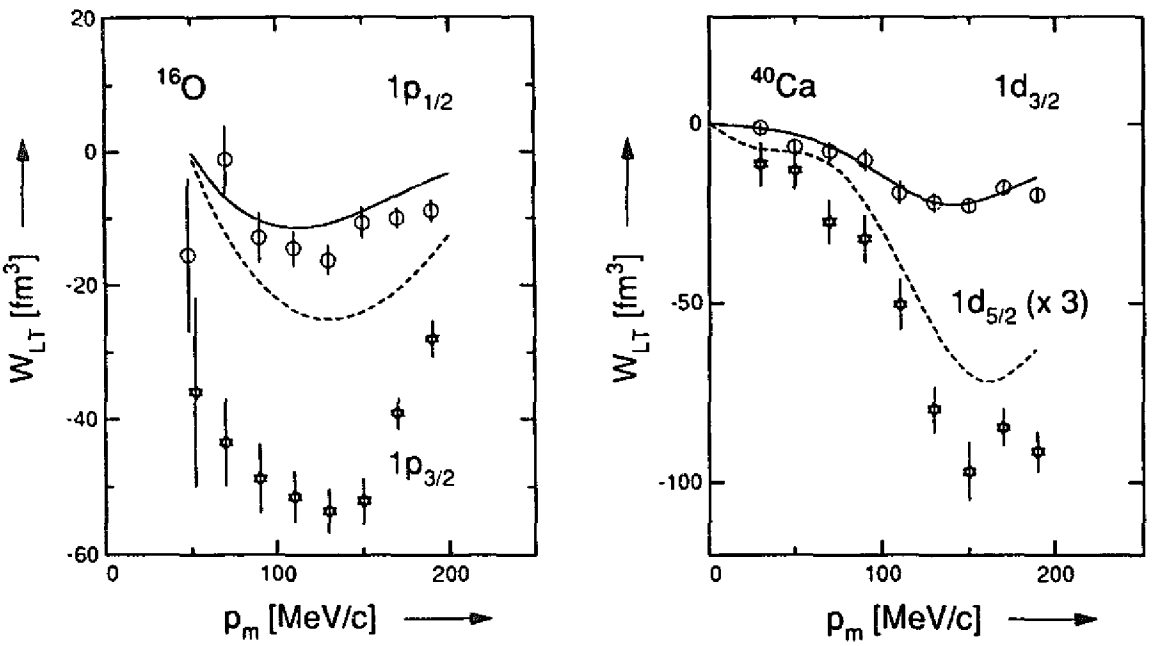

Fig. 5. Longitudinal-transverse structure functions W_{LT} for $1p_{1/2}$ (solid curve, circles) and $1p_{3/2}$ (dashed curves, stars) knockout in the reaction $^{16}O(e,e'p)$ (left, [37]) and for $1d_{3/2}$ (solid, circles) and $1d_{5/2}$ (dashed, stars) knockout in the reaction $^{40}Ca(e,e'p)$ (right, [38]). The curves represent CDWIA calculations with bound-state wave functions and spectroscopic factors determined from fits to data obtained in parallel kinematics.

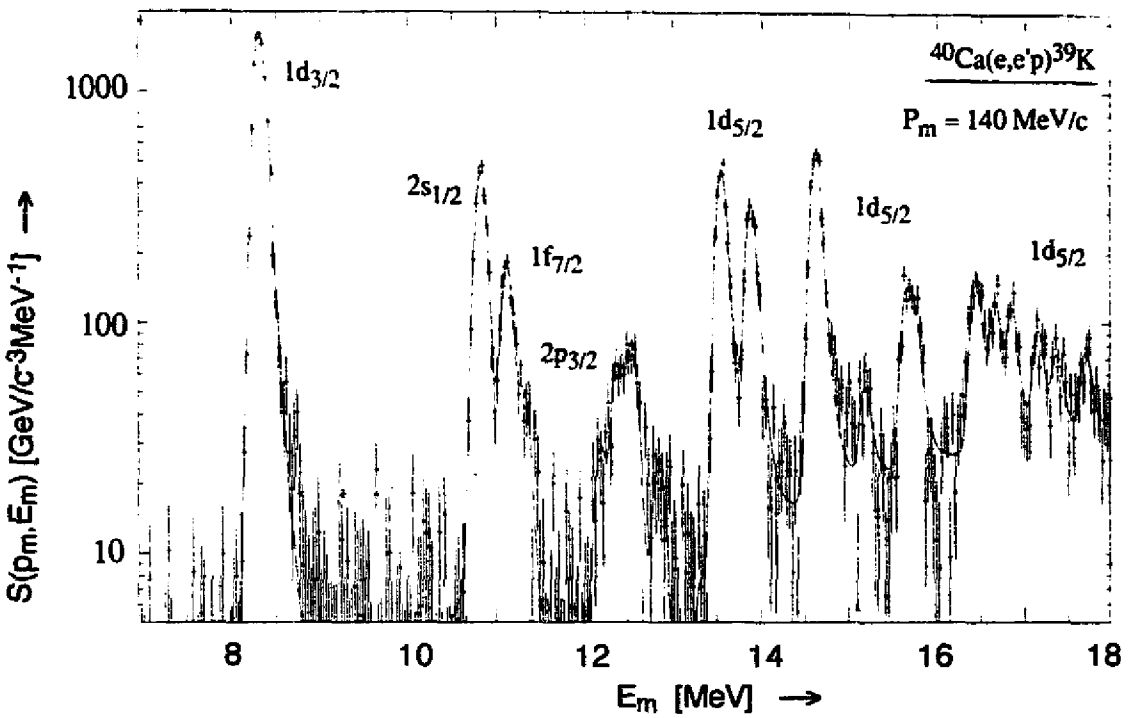

Fig. 6. Missing-energy spectrum of the reaction ^{40}Ca(e,e'p) at p_m= 140 MeV/c showing the knockout of protons from the $1d_{3/2}$, $2s_{1/2}$ and $1d_{5/2}$ orbitals below the Fermi edge and from the $1f_{7/2}$ and $2p_{3/2}$ orbitals above the Fermi edge to discrete states in ^{39}K. The FWHM energy resolution is 100 keV.

4. RESULTS FROM (e,e'p) EXPERIMENTS

4.1 Momentum distributions and mean-field wave functions

At NIKHEF-K high-resolution studies of the (e,e'p) reaction have been carried out for nuclei in the mass range from ^{2}H to ^{209}Bi (see e.g. [43,44] for a survey). Because of the high-resolution (see e.g. fig. 6) transitions to many states in the residual nucleus could be separated and their momentum distributions accurately deduced. A representative sample is given for the closed shell nuclei ^{16}O, ^{40}Ca, ^{90}Zr and ^{208}Pb in fig. 7, which displays momentum distributions for proton knockout from the valence (sub)shell and the next deeper (sub)shell. The curves represent CDWIA calculations in which we employed Woods-Saxon mean-field wave functions whose rms radius was fitted to describe the data. The normalisation of the curves was adapted to obtain the spectroscopic factors for each transition. Fig. 7 clearly shows that the shape of the momentum distributions of transitions to discrete states can be adequately described by mean-field wave functions for momenta up to the Fermi momentum k_F(≈ 250 MeV/c).

This observation is in line with the notion that the experimentally deduced rms radii R_{exp} agree with predictions R_{HF} from Hartree-Fock calculations with a variety of interactions. In fig. 8 we present the relative deviations R_{exp}/R_{HF} -1 as found for Hartree-Fock radii calculated with the G_σ interaction [45]. Nearly all radii are seen to agree within ± 2% with these mean field values and this conclusion holds as well when other interactions of the Skyrme type [45] are employed (see fig. 8). Note that in these mean-field calculations effective forces were used whose parameters were fitted to a number of global observables like binding energies and charge radii. Therefore the observed agreement of the radii for individual orbitals with these mean-field predictions is an implicit consequence of the phenomenological nature of the effective forces.

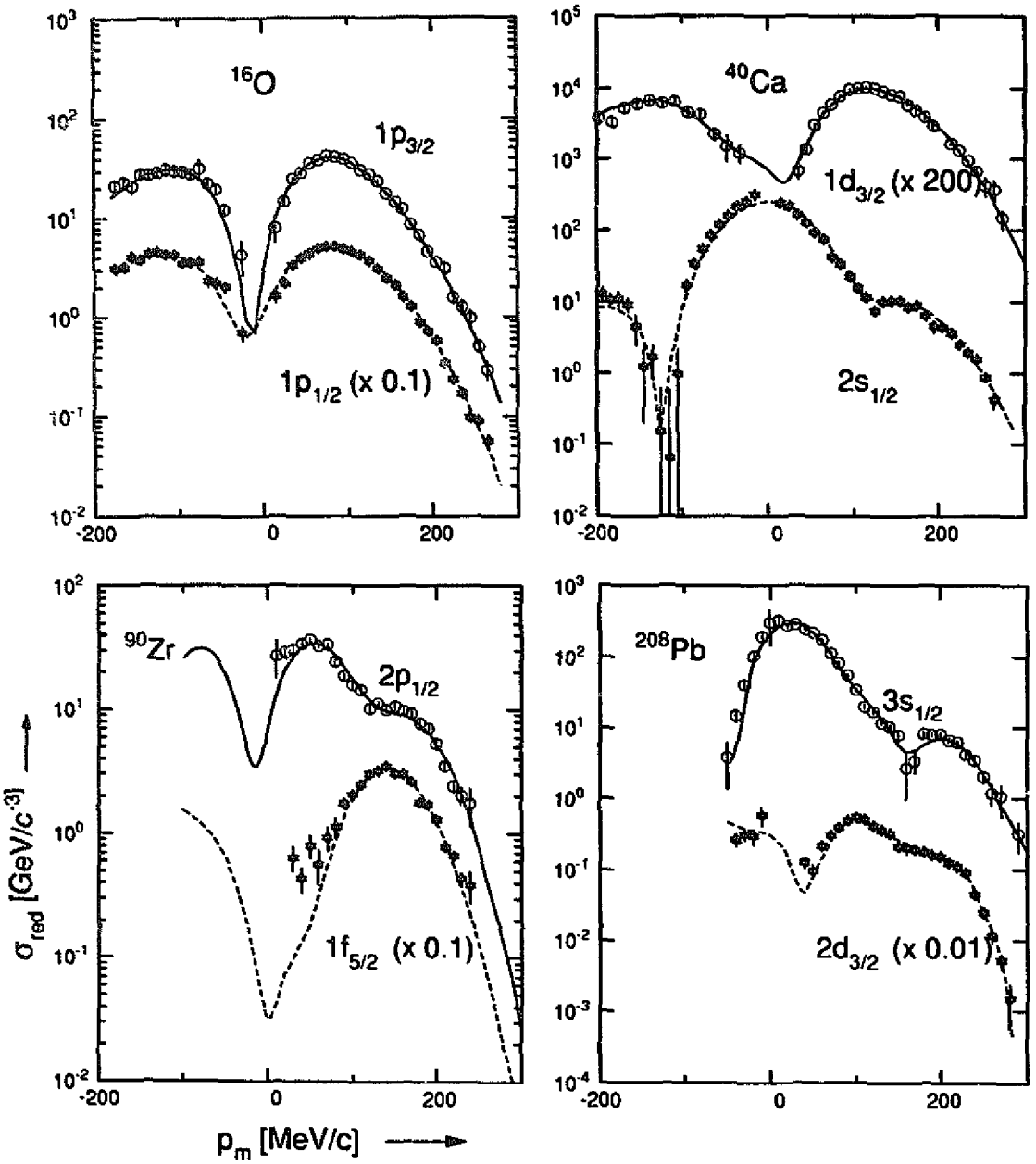

Fig. 7. Experimental momentum distributions for transitions in the reaction (e,e'p) on ^{16}O, ^{40}Ca, ^{90}Zr and ^{208}Pb, involving knockout from the valence shell (upper data) and the next deeper (sub)shell (lower data). The curves represent CDWIA calculations with Woods-Saxon bound-state wave functions of which the spectroscopic factor and rms radius were fitted to the data. The data and curves for some transitions have been scaled as indicated.

4.2 Spectroscopic strengths for orbitals close to the Fermi edge

For the spectroscopic strength the conclusions are quite different, as shown in fig. 9. Here the summed spectroscopic strength $\Sigma S_\alpha/(2j+1)$ for valence orbitals is plotted relative tot the IPSM sum rule (2j+1) as a function of target mass. The strength is integrated over a small energy interval (typically up to 20 MeV) in order to also include fragmentation due to recoupling for non-closed shell nuclei and long-range RPA-type correlations. The average value

for the absolute spectroscopic strength for the studied closed shell nuclei is $\Sigma S_{\alpha \in F}$ = 0.65(5), appreciably lower than the 90 % *occupation* for valence orbitals predicted by Hartree Fock plus RPA theory. A possible explanation for this discrepancy is that sizable short-range and tensor correlations are present, which are not included in the mean-field approximation. Their effect would be twofold. Firstly, they shift strength from the quasi particle peak (see fig. 10) into a tail at large missing energy outside the experimentally accessible domain. Secondly they cause an overall depletion of the states below the Fermi edge and populate the states above it.

The high resolution of the measured (e,e'p) missing energy spectra made it also possible to determine the strength residing in "normally empty" orbitals, i.e. the ones directly above the Fermi edge. In fig. 9 we show the resulting integrated spectroscopic strengths. Their average for closed shell nuclei amounts to $\Sigma S_{\alpha \notin F}$=0.07(3) relative to the IPSM sum rule limit (2j+1). Since the obtained values for the spectroscopic strengths below and above the Fermi edge seem rather mass-independent it is now tempting to compare these results with nuclear matter (NM) calculations.

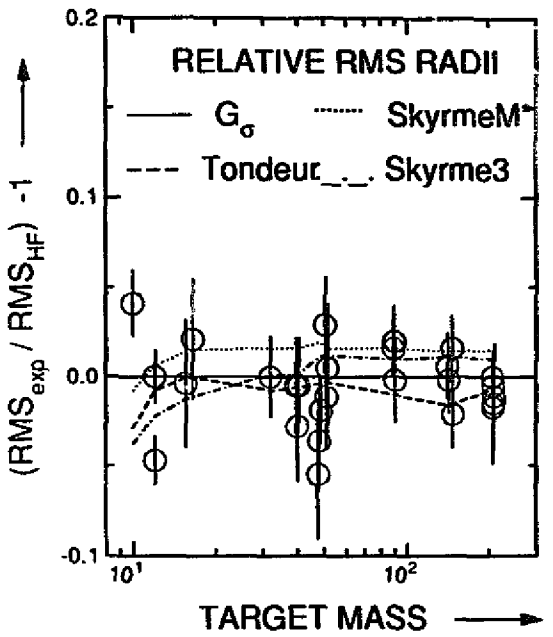

Fig. 8. Relative deviations R_{exp}/R_{HF} -1 for experimental rms radii R_{exp} of valence orbitals as deduced from (e,e'p) data relative to Hartree-Fock radii R_{HF} calculated with the G_σ interaction [45]. The long-dashed, dash-dot and short dashed curves indicate the relative deviations between Hartree-Fock radii obtained with different types of effective interactions (Tondeur, Skyrme 3, Skyrme M*).

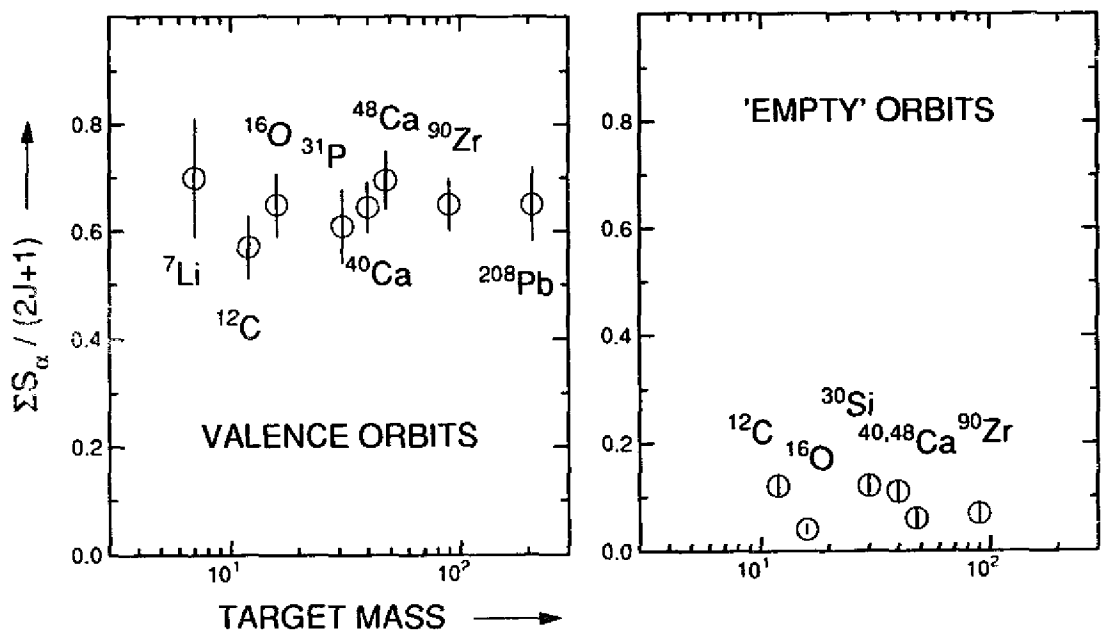

Fig. 9. Quasi-particle strength $\Sigma S_\alpha/(2j+1)$ for valence orbitals (left panel) and for states just above the Fermi edge (right panel), observed in the reaction (e,e'p) as a function of the mass of the target nucleus. All strengths were integrated to an excitation energy of about 20 MeV.

In nuclear matter the relation

$$Z = n_h(k_F\text{-}0) - n_p(k_F\text{+}0), \qquad (4.1)$$

holds between the *occupation* just below ($n_h(k_F\text{-}0)$) and just above ($n_p(k_F\text{+}0)$) the Fermi edge and the *quasi-particle strength* Z. The latter should be identified with $\Sigma S_{\alpha\in F}$= 0.65(5), while a lower limit for $n_p(k_F\text{+}0)$ is given by $\Sigma S_{\alpha\notin F}$=0.07(3). Since most of the particle strength may be assumed to reside in the experimentally covered energy range (see fig. 10) we consider $0.07 \leq n_p \leq 0.15$ a conservative estimate. Hence, we may use these two values and eq. (4.1) to derive the hole occupation for states near the Fermi edge as $n_h(k_F\text{-}0)$ = 0.72-0.80, in agreement with nuclear matter calculations involving realistic potentials [4,5,7,46] that predict $n_h(k_F\text{-}0)$=0.70-0.80. Furthermore the derived value agrees with the one from a combined analysis of elastic electron scattering and (e,e'p) data on nuclei in the lead region [47,50], which results in an *occupation* $n(3s_{1/2})$= 0.75(8) for knockout from the $3s_{1/2}$ orbital in ^{208}Pb.

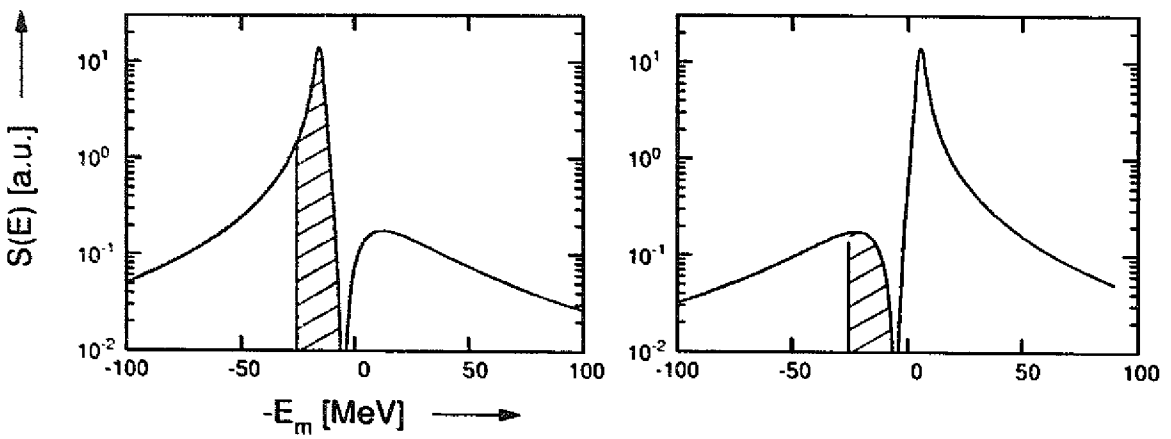

Fig. 10. Energy dependence of the spectral function with the nuclear matter (NM) [49] dependence for the spreading width Γ. The curves were calculated for a hole state located at 15 MeV below the Fermi edge ε_F (left panel) and for a particle state located at 15 MeV above it (right panel). The integral from -∞ to ε_F represents the hole (n_h) or particle occupation (n_p), the integral over the shaded area represents the quasi-hole strength (S) measured in the energy domain covered by the present (e,e'p) experiments. The depletion (1-n) is given by the area under the curve above ε_F. The total area under both curves equals unity.

4.3 Energy dependence of the quasi-particle strength

An interesting question concerns the evolution of the quasi-particle strength as one goes to deeper lying shells. As the NIKHEF experiments covered a limited energy acceptance we could only investigate this dependence for states up to 20 MeV below the Fermi edge. The results for the studied closed-shell nuclei, as obtained from an angular momentum decomposition [32] of the spectral function in the continuum are shown in fig. 11. They closely follow the energy dependence of the quasi-particle strength as predicted by nuclear matter calculations in which a realistic nucleon-nucleon interaction is employed, and to which RPA type corrections were included to account for finite-size effects [4]. It will be of fundamental importance to pursue these experiments out to larger missing energies, since nuclear matter predictions at k=0 predict both Z and n_h to approach a constant value. All calculations employing realistic nucleon-nucleon interactions with a strong short-range repulsion predict $n_h(k_F\text{=}0)\approx$0.83. Experimental determination of the spectral function at large E_m should therefore be carried out for closed-shell nuclei by determining it from an angular momentum decomposition of the (separated) longitudinal structure function, which is known to suffer least from competing processes like multi-nucleon knockout and meson-exchange currents.

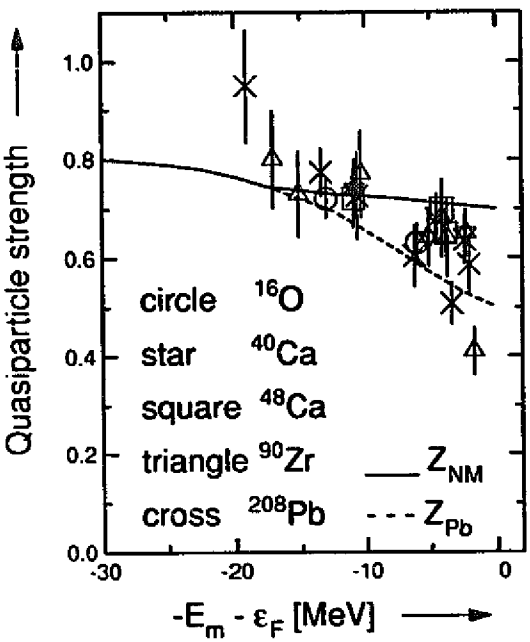

Fig. 11. Summed spectroscopic strength observed for proton knockout from various orbitals in the closed-shell nuclei ^{16}O [41], ^{40}Ca [33,38], ^{48}Ca [33], ^{90}Zr [32] and ^{208}Pb [19,48] as a function of the mean excitation energy of the orbital relative to the Fermi edge. The dashed curve represents the quasi-particle strength calculated for nuclear matter, the solid curve is derived from the nuclear matter curve by including surface effects calculated for ^{208}Pb [4].

5. SUMMARY

Experimental investigations of the validity of the Impulse Approximation in the reaction (e,e'p) have shown that in the Q-range below 500 MeV/c this Ansatz holds well, provided that final-state interactions and two-body currents are properly taken into account. Possible medium modifications of the nucleon form factors should be investigated at higher momentum transfer, as will be feasible with the new generation of CW facilities. At low Q we have observed that the CDWIA framework is not able to describe separated longitudinal-transverse interference structure functions. A thorough investigation of the contributions of meson-exchange currents and the role of a relativistic current operator is called for.

From measurements of the momentum distributions of various orbitals for a range of nuclei by the (e,e'p) reaction, it is concluded that below the Fermi momentum (≈ 250 MeV/c) the these distributions are satisfactorily described by CDWIA calculations with bound state wave functions evaluated in a mean-field potential. However, the spectroscopic strengths for valence orbitals amount to $\Sigma S = 0.6\text{-}0.7$ times the sum rule value (2j+1), to be compared with $\Sigma S \approx 0.9$ for Hartree Fock plus RPA theory. This observed fractional strength for valence orbitals agrees with predictions from nuclear matter calculations that include sizable short-range and tensor correlations. Moreover, the observed energy dependence of the measured quasi-particle strength up to 20 MeV below the Fermi edge agrees with that of the above-mentioned nuclear-matter calculations. This observation should be extended by new measurements of the strength in the deepest-lying orbitals in order to verify the nuclear-matter predictions for the sizable depletion of these orbitals due to short-range correlations. Such measurements, together with those of high-momentum components well above the Fermi momentum, will be possible only with the new generation of CW machines now being commissioned at Amsterdam, Mainz and MIT/Bates.

Acknowledgements

I like to thank W.H. Dickhoff, H.P. Blok and G. van der Steenhoven for stimulating discussions and H.J. Bulten, G.J. Kramer, M.B. Leuschner and H.B.M. Raben for providing data and calculations. This work is part of the research program of the National Institute for Nuclear Physics and High-Energy Physics (NIKHEF) made possible by the financial support from the Foundation for Fundamental Research of Matter (FOM) and the Netherlands' Organization for the Advancement of Research (NWO).

REFERENCES

1. R. Jastrow, Phys. Rev. **98** (1955) 1479.
2. S. Tadokoro *et al.*, Prog. Theor. Phys. **78** (1987) 732.
3. R. Schiavilla *et al.*, Nucl. Phys. **A473** (1987) 267.
4. O. Benhar *et al.*, Phys. Rev. **C41** (1990) R24 and Nucl. Phys. **A505** (1989) 267.
5. B.E. Vonderfecht *et al.*, Nucl. Phys. **A503** (1989) 1.
6. S.C. Pieper *et al.*, Phys. Rev. Lett. **64** (1990) 364.
7. W.H. Dickhoff and H. Müther, Rep. Progr. Phys. **54**(1991) 257.
8. B. Frois and C. Papanicolas, Ann. Rev. Nucl. Sci. **37** (1987) 133.
9. G. Orlandini and M. Traini, Rep. Progr. Phys., to be published.
10. S. Fantoni and V.R. Pandharipande, Nucl. Phys. **A473** (1987) 234.
11. R. Schiavilla *et al.*, Nucl. Phys. **A473** (1987) 290.
12. V.R. Pandharipande *et al.*, Phys. Rev. Lett. **53** (1984) 1133.
13. C.N. Papanicolas and S.E. Williamson, Proc. Int. Conf. on the Spectroscopy of Heavy Nuclei, Crete, 1989.
14. C. Marchand *et al.*, Proc. this conference.
15. J.E. Ducret *et al.*, Proc. this conference.
16. S. Frullani and J. Mougey, Adv. Nucl. Phys. **14** (1984) 1.
17. T. de Forest Jr, Nucl. Phys. **A329** (1983) 232.
18. C. Giusti and F. Pacati, Nucl. Phys. **A485** (1988) 461.
19. J.P. McDermott, Phys. Rev. Lett. **65** (1990) 1991.
20. P.J. Mulders, Nucl. Phys. **A459** (1986) 525 and Phys. Rep. **185** (1990) 83.
21. M. van der Schaar *et al.*, Phys. Rev. Lett. **66** (1991) 2855.
22. G. van der Steenhoven *et al.*, Phys. Rev. Lett. **58** (1987) 1727.
23. J.B.J.M. Lanen *et al.*, Phys. Rev. Lett. **64** (1990) 2250.
24. G. van der Steenhoven *et al.*, Phys. Rev. Lett. **57** (1986) 182.
25. H.J. Bulten, Ph. D. Thesis, State University Utrecht, 1992.
26. S. Boffi and M. Radici, Nucl. Phys. **A256** (1991) 602.
27. P.E. Ulmer *et al.*, Phys. Rev. Lett. **59** (1987) 2259.
28. G. van der Steenhoven *et al.*, Nucl. Phys. **A480**(1988) 547.
29. A. Magnon *et al.*, Phys. Lett. **B222**(1989) 352.
30. M. Buballa *et al.*, Phys. Rev. **C44** (1991) 810.
31. J.F.J. van den Brand, Ph. D. Thesis, University of Amsterdam, 1988.
32. J.W.A. den Herder *et al.*, Nucl. Phys. **A490** (1988) 507.
33. G.J. Kramer, PhD thesis, University of Amsterdam, 1990.
34. J.P. Ralston and B. Pire, Nucl. Phys. **A532**(1991) 155c.
35. L. Chinitz *et al.*, Phys. Rev. Lett. **67** (1991) 568.
36. M. van der Schaar *et al.*, Phys. Rev. Lett. **68** (1992) 776.
37. C. Spaltro, Master's Thesis, State University Utrecht, 1992 (unpublished).
38. H.B.M. Raben and H.P. Blok, to be published
39. W. Fabian and H. Arenhövel, Nucl. Phys. **A314** (1979) 253
40. E. Hummel and J.A. Tjon, Phys. Rev. Lett. **63** (1989)1788 , Phys. Rev. **C42** (1990) 423
41. M.B. Leuschner *et al.*, to be published.
42. B. Mosconi and P. Ricci, Nucl. Phys. **A517**(1990) 483.
43. P.K.A. de Witt Huberts, Journ. Phys. **G16** (1990) 507.
44. A.E.L. Dieperink and P.K.A. de Witt Huberts, Ann. Rev. Nucl. Part. Sci. **40** (1990) 239.
45. J. Friedrich and P.-G. Reinhard, Phys. Rev. **C33** (1986) 335.
46. M. Baldo *et al.*, Phys. Rev. **C41** (1990) 1748.
47. P. Grabmayr, Prog. Part. Nucl. Phys. **29**(1992) 251.
48. E.N.M. Quint, Ph. D. Thesis, University of Amsterdam, 1988.
49. J.P. Jeukenne, A. Lejeune and C. Mahaux, Phys. Rep. **25C** (1976) 83.
50. I. Sick and P.K.A. de Witt Huberts, Comm. Nucl. Part. Phys. **20** (1991)177.